Earth Planets Space, **56**, 955–966, 2004

Application of satellite magnetic observations for estimating near-surface magnetic anomalies

Hyung Rae Kim[1], Ralph R. B. von Frese[2], Alexander V. Golynsky[3], Patrick T. Taylor[4], and Jeong Woo Kim[5]

[1]*Goddard Earth Science and Technology Center (GEST), University of Maryland, Baltimore County and Code 921, Goddard Space Flight Center/NASA, Greenbelt, Maryland 20771, USA*
[2]*Department of Geological Sciences and Byrd Polar Research Center, The Ohio State University, Columbus, Ohio 43210, USA*
[3]*VNIIOkeangeologia, St. Petersburg 190121, Russia*
[4]*Geodynamics Branch, NASA Goddard Space Flight Center, Greenbelt, Maryland 20771, USA*
[5]*Department of Geoinformation Engineering, Sejong University, Seoul 143-747, Korea*

(Received January 12, 2004; Revised August 14, 2004; Accepted September 1, 2004)

Regional to continental scale magnetic anomaly maps are becoming increasingly available from airborne, shipborne, and terrestrial surveys. Satellite data are commonly considered to fill the coverage gaps in regional compilations of these near-surface surveys. For the near-surface Antarctic magnetic anomaly map being produced by the Antarctic Digital Magnetic Anomaly Project (ADMAP), we show that near-surface magnetic anomaly estimation is greatly enhanced by the joint inversion of the near-surface data with Ørsted satellite observations compared to Magsat data that have order-of-magnitude greater measurement errors, albeit collected at much lower orbital altitudes. The CHAMP satellite is observing the geomagnetic field with the same measurement accuracy as the Ørsted mission, but at the lower orbital altitudes covered by Magsat. Hence, additional significant improvement in predicting near-surface magnetic anomalies can result as lithospheric magnetic anomaly data from the CHAMP mission become available. Our analysis also suggests that a further order-of-magnitude improvement in the accuracy of the magnetometer measurements at minimum orbital altitude may reveal considerable new insight into the magnetic properties of the lithosphere.

Key words: Crustal magnetic anomaly, satellite data, ADMAP, least squares inversion.

1. Introduction

Considerable efforts have been made to isolate and verify the crustal magnetic anomaly field from Earth-orbiting satellite magnetometer measurements (e.g., Regan *et al*., 1975; Langel *et al*., 1982; Langel, 1990; Cohen and Achache, 1990; Arkani-Hamed *et al*., 1994; Alsdorf *et al*., 1994; Ravat *et al*., 1995; Maus *et al*., 2002). In general, crustal anomaly maps at satellite altitudes can be interpreted only for regional geologic features. However, for insight into the smaller scale magnetic geology, satellite altitude anomalies are typically downward continued to or near the Earth's surface. Additional insights can also result from comparing satellite altitude anomalies with upward continued magnetic anomaly surveys of the near-surface. Upward continuation transforms potential field anomalies to elevations further away from the sources and is a stable operation, while downward continuation is an unstable, noise-amplifying transformation of the anomalies towards the sources.

These continuations are commonly based on either global or local representations of the magnetic anomalies. For example, satellite altitude magnetic observations are often modeled using spherical harmonic expansions (e.g., Arkani-Hamed and Strangway, 1985; Arkani-Hamed *et al*., 1985; Arkani-Hamed *et al*., 1994; Ravat *et al*., 1995; Maus *et al*., 2002). However, these models require global data sets that may incorporate substantial data errors due to the uneven quality of the data measurements and their reductions for core and external field components over different regions of the Earth. Hence, the downward continuation of satellite magnetic anomalies from spherical harmonic expansions can be limited by the enhancement of these data errors in the near-surface predictions.

Local representations from equivalent source models (e.g., Dampney, 1969; Mayhew, 1982; von Frese *et al*., 1981b; Purucker *et al*., 1996; von Frese, 1998) can more fully account for the local data qualities and errors in the magnetic observations. Excepting the long wavelength magnetic anomalies over Canada (Arkani-Hamed *et al*., 1995; Pilkington and Roest, 1996; Ravat *et al*., 2002), however, comparisons of downward continued satellite magnetic anomalies with near-surface survey data, or upward continued near-surface survey anomalies with satellite anomalies have mostly yielded poorly correlated and inconsistent results (e.g., von Frese *et al*., 1982; Sexton *et al*., 1982; Schnetzler *et al*., 1985; Grauch, 1993; Whaler, 1994; Ravat *et al*., 1998).

Figure 1 shows an example of the inconsistencies of continuing individual anomaly fields over great altitude differences. This example considers independently mapped aeromagnetic data low-passed filtered for roughly 400 km and larger anomalies and Magsat magnetic anomalies over Kursk, Russia that are associated with massive quartz iron-ore formations (Taylor *et al*., 2003). Comparing these maps

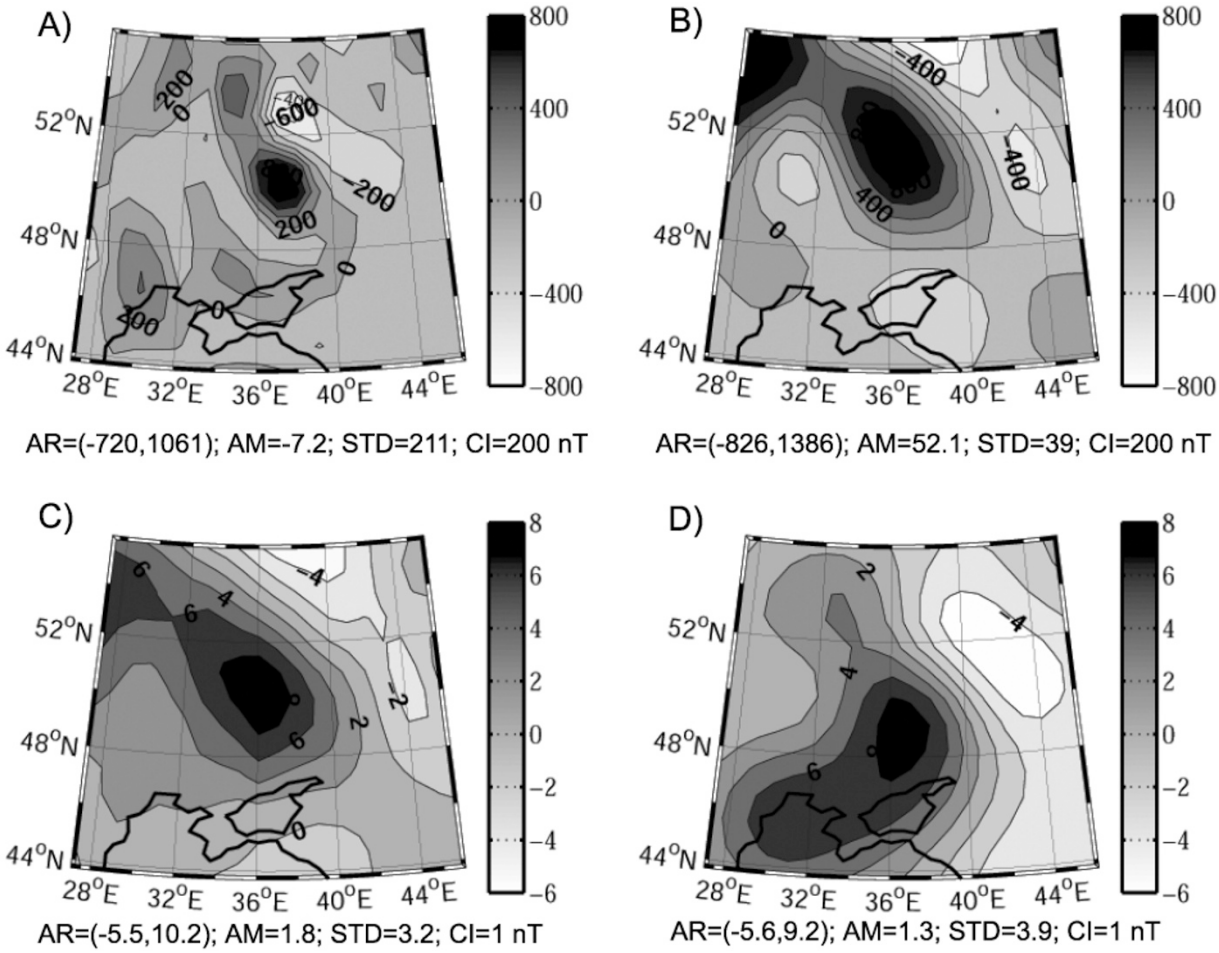

Fig. 1. Comparison of single-field continuations of regional aeromagnetic (A) and Magsat (B) magnetic anomalies at respective altitudes (Z) of 2 km (A, B) and 400 km (C, D) centered on Kursk, Russia. Equivalent point dipole inversion was used to downward continue the Magsat data to 2 km (C) and upward continue the aeromagnetic data to 400 km (D) in spherical Earth coordinates. Grid spacing was approximately 100 km for the individual maps. Statistics given for the anomaly maps include the amplitude range (AR) of (min, max)-values, the amplitude mean (AM), standard deviation (STD) and the contour interval (CI). Correlation coefficients between the satellite and aeromagnetic anomaly maps are 0.3 at 2 km and 0.6 at 400 km.

and their statistics shows that both the upward and downward continuations are relatively marginal in representing the amplitude and phase properties of the observed magnetic anomalies.

The mismatch in the continuations of independently observed magnetic anomaly data sets can reflect a variety of factors including data measurement and reduction errors. These factors may conspire, for example, to greatly limit or totally negate the sensitivity of satellite altitude measurements for the relatively weak magnetic effects of shallow crustal sources that at the near-surface integrate into strong regional anomaly patterns (e.g., von Frese *et al*., 2004). On the other hand, measurement and data reduction errors can strongly bias the near-surface anomalies to the regional effects of the shallow sources at the expense of the deeper crustal source effects that may predominate at satellite altitudes. Thus, the different biases of satellite and near-surface observations for the disparate anomaly interference effects can greatly complicate matching the magnetic anomaly fields by simple single surface continuations. These biases may also contribute to the apparent lack of spectral overlap in the 400–900 km range of anomaly wavelengths that has been observed between individually continued satellite and near-surface magnetic anomaly fields (Grauch, 1993; Whaler, 1994; Hildenbrand *et al*., 1996; Langel and Hinze, 1998).

Hence, in the absence of measurements in the intervening altitudes to constrain the nonunique continuation estimates, there seems to be little recourse but to consider the continuations of these anomalies in the context of anomaly models that jointly satisfy both the satellite and near-surface measurements. This joint inversion approach was initially implemented over Canada by weighting the satellite and aeromagnetic anomalies to adjust the inversion for the different survey error levels (Ravat *et al*., 1998, 2002). However, simple unweighted inversions of near-surface and satellite magnetic anomalies have also yielded geologically plausible results, such as for the Weddell Sea region of Antarctica where magnetic anomaly error levels were poorly constrained at all altitudes (von Frese *et al*., 1999a).

In this paper, we investigate the utility of the joint inversion of satellite and available near-surface magnetic data for augmenting regional gaps in coverage in near-surface anomaly compilations of terrestrial, airborne, and shipborne magnetic surveys. The nature of the problem is shown by the near-surface magnetic anomalies that were compiled by the Antarctic Digital Magnetic Anomaly Project (ADMAP)

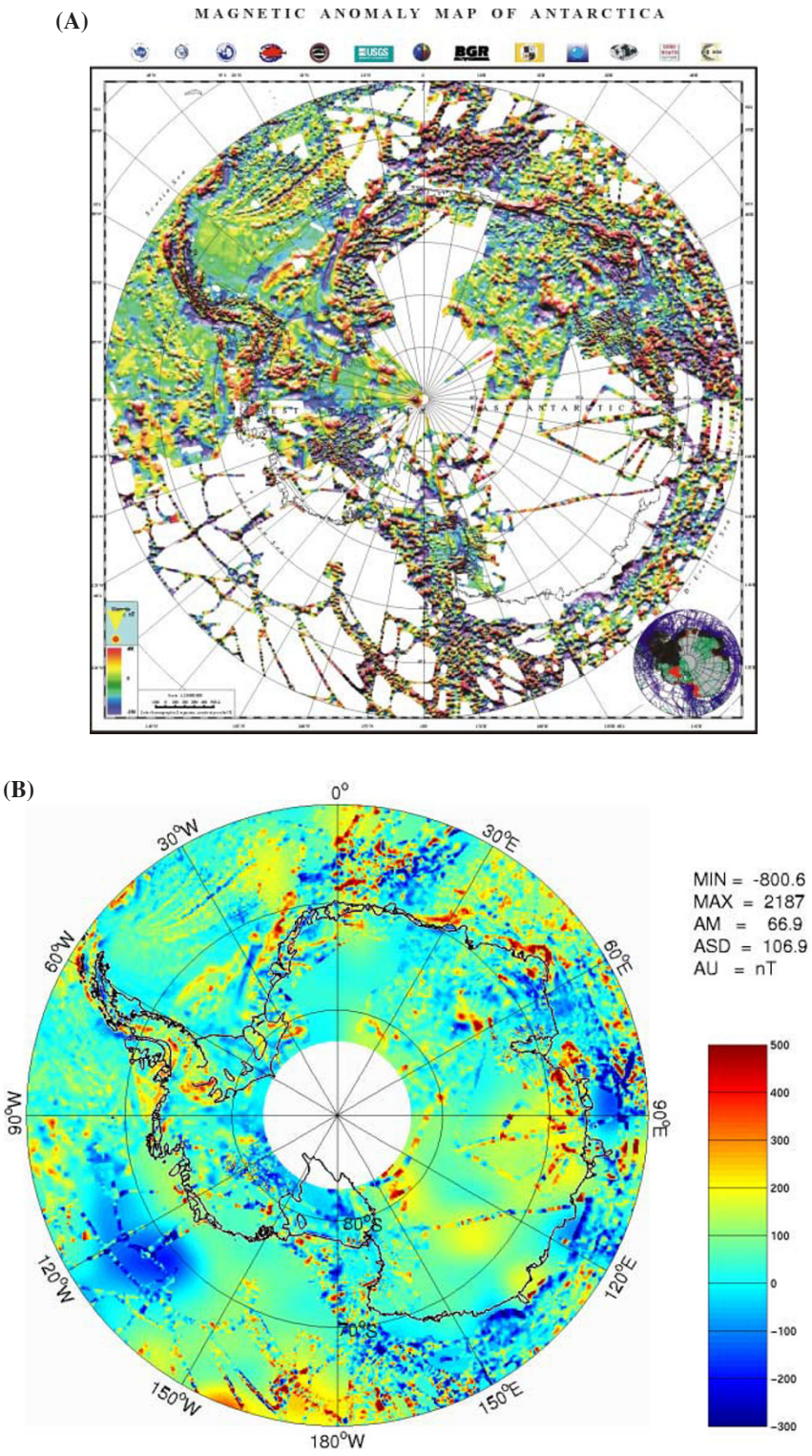

Fig. 2. (A) Near-surface magnetic anomalies of the Antarctic from ADMAP (Golynsky *et al.*, 2002). (B) Antarctic magnetic anomaly map at 5 km altitude that includes the superposition of the Ørsted-based predictions of Fig. 8(A) and the ADMAP anomalies high-pass filtered for wavelengths smaller than roughly 400 km.

in Fig. 2(A) (Golynsky *et al.*, 2002). Only satellite magnetic observations are available at present to constrain anomaly estimates in these coverage gaps.

The available satellite magnetic data reflect disparate measurement accuracies and mission parameters that affect the utility of the various missions for augmenting near-surface magnetic survey data. The Magsat mission, for example, obtained data over 350–550 km altitudes with roughly 3–6 nT measurement accuracies (Langel and Hinze, 1998). However, this short 7-month mission was flown over Austral summer and fall when external field activity over the Antarctic was relatively severe and disruptive of the core and lithospheric geomagnetic components. The new multi-year Ørsted and CHAMP missions, by contrast, include min-

imally disturbed Austral winter observations with an order-of-magnitude improvement in measurement accuracy (~0.3 nT). However, the observational altitudes of the new generation missions are vastly different, with Ørsted operating over 650–850 km orbits while CHAMP is providing data over 300–450 km elevations.

In the sections below, we develop an approach for using the satellite magnetic data to fill-in coverage gaps in the near-surface data based on the joint inversion of the two data sets. Specifically, we use simulations to study the relative utilities of the Magsat, Ørsted, and CHAMP observations for this application. In our simulations, we invoke the ideal condition of no anomaly reduction errors so that the anomaly errors reflect only the measurement accuracy of each mission. Our analysis finds that the CHAMP data will be particularly suitable because the measurement errors are an order-of-magnitude smaller than Magsat's and the orbital altitudes are much lower than Ørsted's. We also develop and contrast magnetic anomaly estimates for the ADMAP coverage gaps from the Ørsted comprehensive lithospheric magnetic anomalies (Kim, 2002).

2. Magnetic Anomaly Inversion

Effective inversion requires an appropriate representation or forward model for the regional magnetic anomalies. Accordingly, we consider the regional anomalies in terms of the magnetic effects of crustal prisms using Gauss-Legendre quadrature integration (von Frese *et al.*, 1981a). Specifically, the total magnetic effect (ΔT) in spherical coordinates (r, θ, ϕ) of a crustal prism with uniform intensity of magnetization Δs may be evaluated by:

$$\Delta T(r,\theta,\phi) \approx \Delta\phi_l' \sum_{l=1}^{nl}\{\Delta\theta_j' \sum_{j=1}^{nj}(\Delta r_i' \sum_{i=1}^{ni}[-\mathbf{u}\cdot\nabla \cdot\left\{\mathbf{u}'\cdot\nabla'\left(\frac{1}{R}\right)\right\}\Delta s]A_i r_i'^2)A_j \sin\theta_j'\}A_l, \quad (1)$$

where R is the distance between the source-point coordinates (primed) and observation-point coordinates (unprimed), $\mathbf{u}'$ is the unit vector in source coordinates (r', θ', ϕ'); $\mathbf{u}$ is the unit vector in observation coordinates (r, θ, ϕ); (∇', ∇) are the gradient operators in source and observation point coordinates, respectively; and (A_i, A_j, A_l) are the Gauss-Legendre quadrature weights (Stroud and Secrest, 1966). In addition, $\Delta\phi_l' = [(\phi_{la}' - \phi_{lb}')/2]$, $\Delta\theta_j' = [(\theta_{ja}' - \theta_{jb}')/2]$, and $\Delta r_i' = [(\Delta r_{ia}' - \Delta r_{ib}')/2]$, where (ϕ_{la}', ϕ_{lb}'), $(\theta_{ja}', \theta_{jb}')$, and (r_{ia}', r_{ib}') are the lower (a) and upper (b) boundaries of the prism, respectively, in the l-th coordinate of longitude (ϕ), the j-th coordinate of co-latitude (θ), and i-th radial coordinate (r). Note that in the crustal model we can adjust $\mathbf{u}'$ and Δs for each prism to account for variations of crustal magnetization. Similarly, we can adjust $\mathbf{u}$ at each observation point to accommodate the inclination and declination variations of the core field.

By Eq. (1), the magnetic anomaly due to a spherical prism is evaluated by summing at each observation point the anomalous effects of $nl \times nj \times ni$ equivalent point dipoles (von Frese *et al.*, 1981b; von Frese, 1998). Here, each differential point source anomaly is appropriately weighted by Gauss-Legendre quadrature coefficients and the volume coordinate limits of the anomalous body being modeled. The accuracy of the solution depends on the number of nodes or point sources within the prism used in the integration. In particular, maximum accuracy is obtained when the distance between the point sources (i.e., the node spacing) is smaller than the distance to the observation point (Ku, 1977; von Frese *et al.*, 1981a).

Now, the linear least squares inversion problem for regional magnetic anomalies can be generalized in matrix notation by:

$$\mathbf{AX} = \mathbf{B}. \quad (2)$$

Here, the $n \times m$ coefficients of the design matrix $\mathbf{A}$ for any specified distribution of crustal prisms are completely determined in Eq. (1) by setting $\Delta s = 1$, while $\mathbf{X}$ is the $m \times 1$ column matrix containing the solution of magnetization intensities for the prisms, and $\mathbf{B}$ is an $n \times 1$ column matrix of the magnetic anomaly observations. Hence, the least squares solution of Eq. (2) can be simply calculated by:

$$\mathbf{X} = [\mathbf{A}^{\mathrm{T}}\mathbf{A}]^{-1}\mathbf{A}^{\mathrm{T}}\mathbf{B}. \quad (3)$$

In practice, errors in computing the coefficients in $\mathbf{A}$ due to limitations of the forward modeling algorithm and the computer's working precision may yield an unstable solution $\mathbf{X}$ with large and erratic values, and hence large variance. In this case, the solution can be useless for predicting anything other than the original observations in $\mathbf{B}$. To obtain a more stable and better performing solution, we commonly evaluate the system in Eq. (2) for the damped least squares solution given by:

$$\mathbf{X} = [\mathbf{A}^{\mathrm{T}}\mathbf{A} + (\mathrm{EV})\mathbf{I}]^{-1}\mathbf{A}^{\mathrm{T}}\mathbf{B}, \quad (4)$$

where $\mathbf{I}$ is the identity matrix, and the scalar EV is variously called the damping factor, Marquardt parameter, or error variance (e.g., von Frese *et al.*, 1988). The damped least squares approach requires choosing an EV-value that is just large enough to stabilize the solution for meaningful predictions (e.g., anomaly continuation, interpolation, etc.), yet still small enough to maintain an acceptable match to the observations $\mathbf{B}$. In any application, we can construct trade-off diagrams that are very effective for determining an "optimal" EV-value. As described in Section 3.1 below, the diagrams compare the statistical properties of the predictions against the errors of fit to the observations for solutions obtained from a range of EV-values (von Frese *et al.*, 1988; Ravat *et al.*, 1991).

3. Near-Surface Magnetic Anomaly Simulations

To test the use of satellite magnetic data to fill-in coverage gaps in near-surface surveys, we constructed a model of crustal magnetization variations for controlling the anomaly estimates from 5 km to satellite altitudes. We developed the model to conform to the regional components of Fig. 3(A), which shows the near-surface ADMAP magnetic anomalies of the Weddell Sea sector. We low-pass filtered these anomalies for 400 km and larger wavelength components that are likely to be detected at satellite altitudes of 400 km and higher (Ravat *et al.*, 2002).

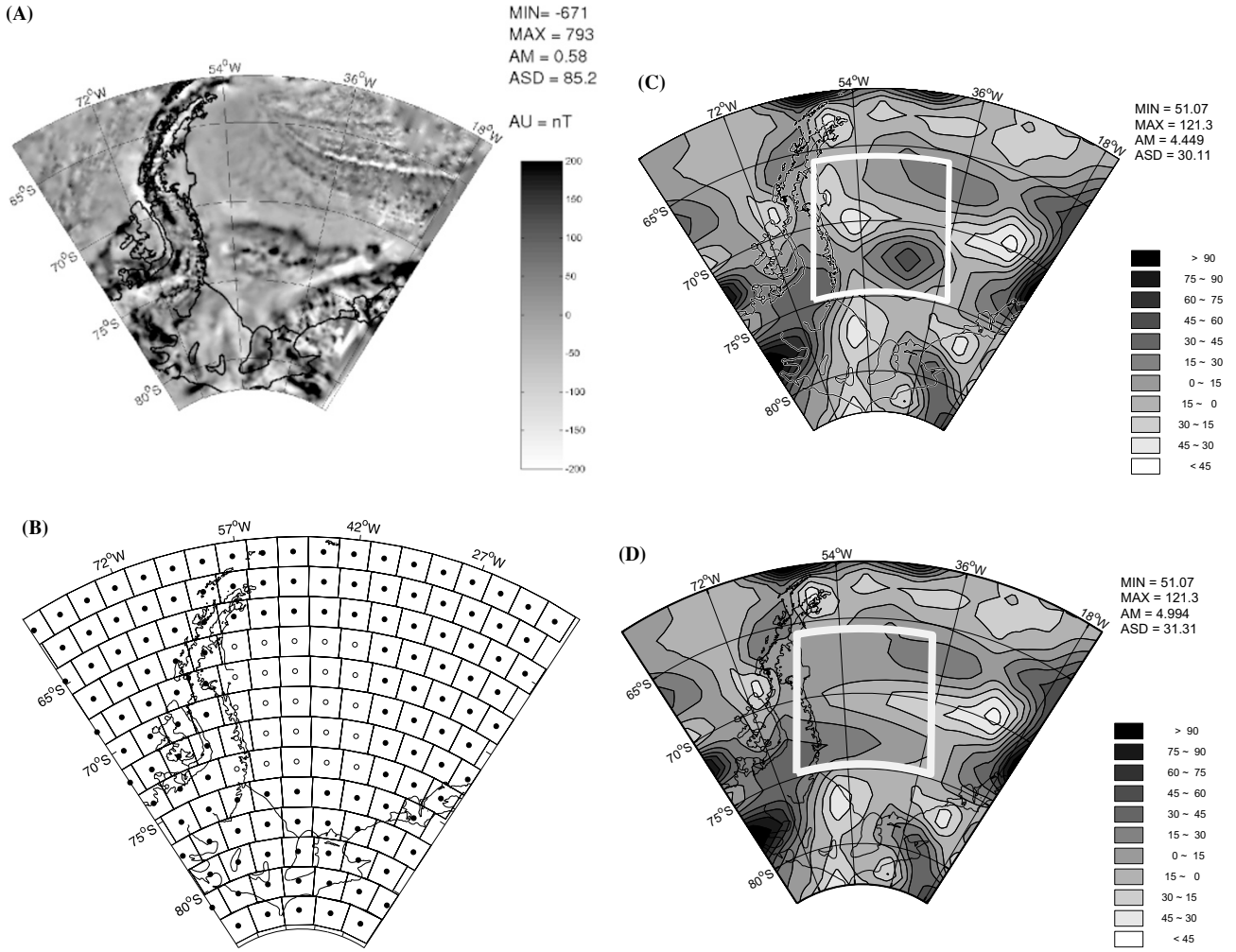

Fig. 3. (A) ADMAP aeromagnetic anomalies (nT) over the Weddell Sea at 5 km above sea level. The grid interval for these anomalies is 10 km. (B) Distribution of spherical crustal prisms with the dots delineating the simulated coverage. Empty dots mark the locations at which we seek effective magnetic anomaly predictions. (C) Simulated aeromagnetic anomalies from the spherical prism model of crustal magnetizations obtained by inversion of the ADMAP anomalies low-pass filtered for 400 km and larger wavelengths. The anomalies that our simulations seek to estimate are within the white-bordered area. (D) Minimum curvature predictions of the regional magnetic anomalies in the gap. Listed attributes for the anomaly maps include the minimum (MIN) and maximum (MAX) amplitudes, the amplitude mean (AM), amplitude standard deviation (ASD), amplitude unit (AU), and map altitude (Z).

We then used damped least squares matrix inversion to relate the low-pass filtered anomalies to the induced magnetization contrasts of an array of crustal prisms across the study area modeled by spherical coordinate Gauss-Legendre quadrature integration. For the inversion, we assumed the low-pass filtered anomalies at 5 km altitude and dimensioned each prism 150 km on side, and 20 km thick with its top prism at 30 km below sea level. The aeromagnetic effect of each prism was evaluated at 5 km above sea level using an $nl \times nj \times ni = 32 \times 32 \times 8$ equivalent point dipole quadrature formula. Here, we used the Ørsted99c core field model (Olsen *et al*., 2000) to set the core field attitudes of the unit vectors $\mathbf{u}'$ and $\mathbf{u}$ in Eq. (1). The inversion effectively solved for the volume magnetic susceptibility Δk of each prism assuming the magnetization intensity contrast is given by $\Delta s = \mathrm{Fe}\Delta k$, where Fe is the inducing field intensity from the core field model.

Figure 3(C) gives the magnetic anomaly predictions at 5 km altitude from the crustal prisms with magnetic effects that matched the input low-pass filtered magnetic anomalies with negligible error. Figure 3(B) shows the locations of the simulated regional aeromagnetic observations at 5 km altitude, as well as the crustal prisms used for the anomaly inversions.

With this inversion model, we now consider the problem of estimating near-surface anomaly values within the coverage hole or gap outlined by the white border in Fig. 3(C) at the locations marked by the open circles in Fig. 3(B). For example, Figure 3(D) shows the anomaly predictions from a conventional interpolation of the near-surface data by minimum curvature (Briggs, 1974; Smith and Wessel, 1990). The interpolated values compare relatively poorly to the 'true' values of Fig. 3(C). Table 1 also lists quantitative measures of the fit that include the root-mean-squared (RMS) difference and correlation coefficient (CC) between the 'predicted' and 'true' anomaly values within the gap.

To test the use of satellite magnetic observations to predict the near-surface anomalies within the coverage gap, we evaluated our crustal prism model for simulated satellite anomalies using the disparate observation parameters of these mis-

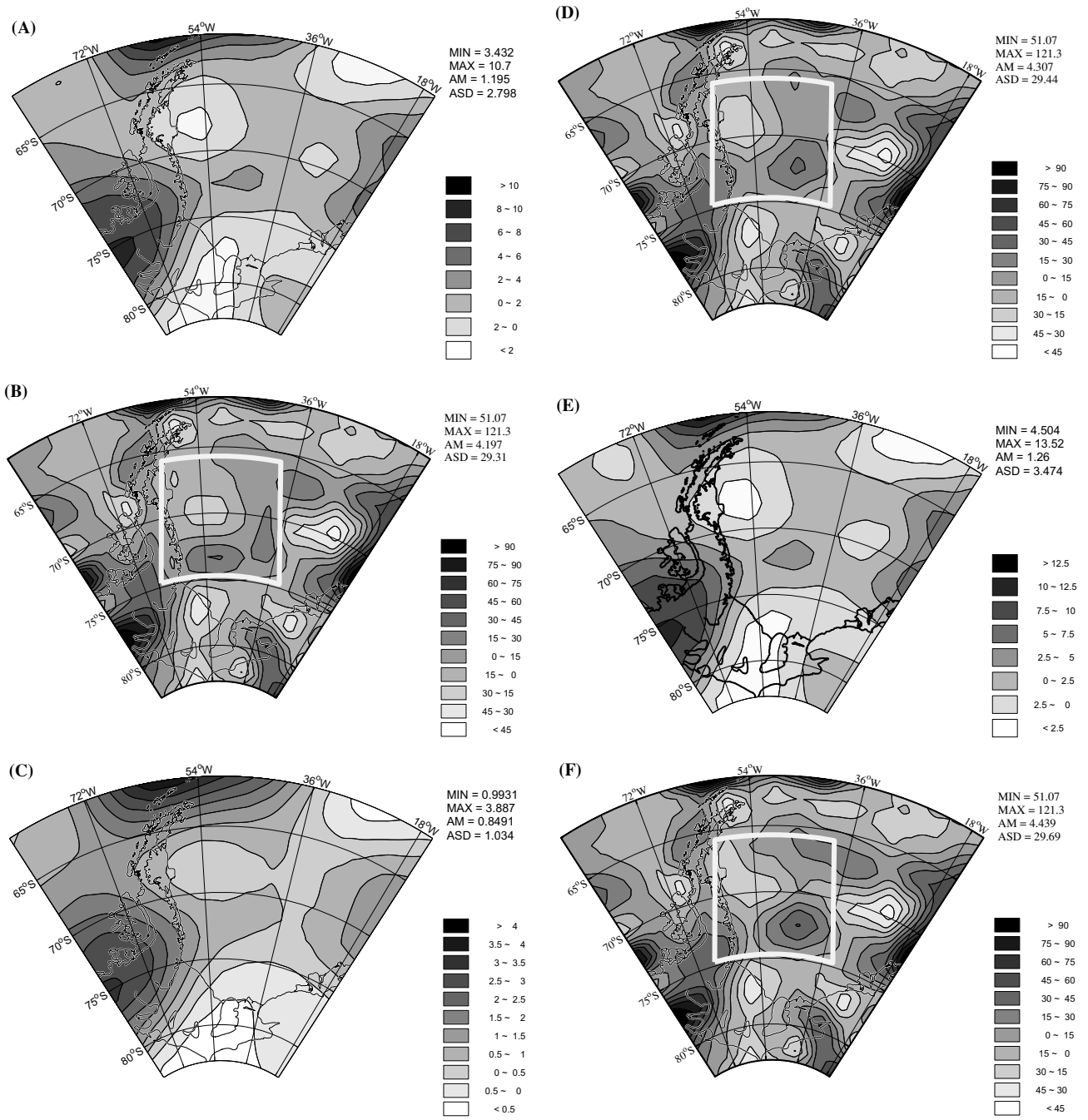

Fig. 4. (A) Simulated Magsat anomalies at 400 km altitude with 3 nT errors. (B) Near-surface magnetic anomaly estimates at 5 km altitude for the coverage gap (white bordered area) by joint inversion of simulated near-surface anomaly data outside the gap and Magsat anomaly simulations at 400 km altitude. (C) Simulated Ørsted anomalies at 700 km altitude with 0.3 nT errors. (D) Near-surface magnetic anomaly estimates at 5 km altitude by joint inversion with Map C. (E) Simulated CHAMP anomalies at 350 km altitude with 0.3 nT errors. (F) Near-surface magnetic anomaly estimates at 5 km altitude by joint inversion with Map E.

sions. Figure 4(A), for example, gives our simulated Magsat anomalies at 400 km altitude that we evaluated from the inversion model to the nearest 3 nT to simulate the magnetometer measurement errors. Maximum accuracy in modeling the satellite altitude magnetic effects was achieved using an $nl \times nj \times ni = 4 \times 4 \times 4$ equivalent point dipole quadrature formula for each crustal prism. We then obtained gap predictions by joint inversion of the simulated satellite anomalies with the near-surface anomalies outside the gap located at the positions marked by the black dots in Fig. 3(B). Details for the joint inversion of these magnetic anomalies are given in the next section.

3.1 Joint inversion of magnetic anomalies

The term "joint inversion" in geophysics refers to the inversions of independently observed data sets (e.g., Ravat *et al.*, 1998, 2002; Li and Oldenburg, 1990; von Frese *et al.*, 1999a). For this application, the design matrix is given by $\mathbf{A} = [\mathbf{A}_{aero} \quad \mathbf{A}_{sat}]^{\mathrm{T}}$, where $\mathbf{A}_{aero}$ and $\mathbf{A}_{sat}$ are submatrics of respective orders $(n_{aero} \times m)$ and $(n_{sat} \times m)$ that reflect the geometric relationships between the crustal prism source coordinates and the respective aeromagnetic and satellite observation coordinates. Additionally, the observation vector

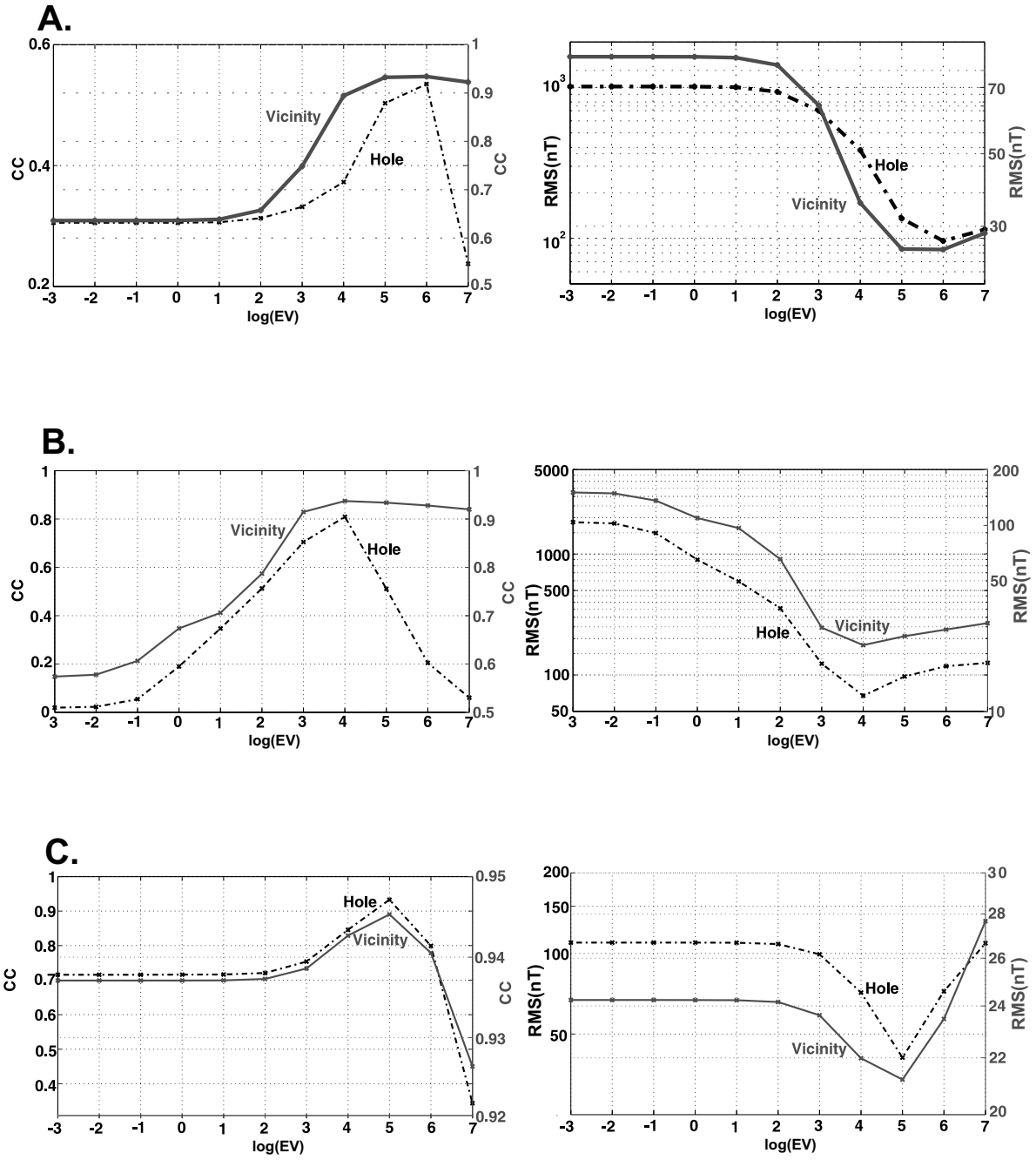

Fig. 5. (A) Magsat trade-off diagrams for obtaining an "optimal" value of error variance (EV) in terms of the correlation coefficient (CC) and RMS difference of the predictions within the hole (dashed dark lines referring to the left vertical axes) and the surrounding vicinity (solid gray lines referring to the right vertical axes). (B) Ørsted trade-off diagrams and RMS difference of the predictions within the hole. (C) CHAMP trade-off diagrams and RMS difference of the predictions within the hole.

$\mathbf{B} = [\mathbf{B}_{aero}\ \mathbf{B}_{sat}]^{\mathrm{T}}$ includes the subvectors $\mathbf{B}_{aero}$ and $\mathbf{B}_{sat}$ of respective orders $(n_{aero} \times 1)$ and $(n_{sat} \times 1)$ that represent the aeromagnetic and satellite magnetic anomaly observations, respectively.

The accuracy of the anomaly estimates for the coverage gaps obtained by joint inversion from Eq. (4) is controlled by the accuracy of the input anomaly data and the choice of the error variance (EV). Input magnetic anomaly errors largely result from anomaly reduction errors due to inaccurate estimates of the core and external field components in the magnetometer measurements, whereas the magnetometer measurement errors control the minimum size of the input anomaly errors. For our simulations, we assumed the optimal condition of minimum input anomaly errors by evaluating all anomalies to the nearest value that each satellite magnetometer measured. However, to obtain the most effective anomaly predictions in each coverage gap, we established trade-off diagrams to find the "optimal" EV-value and solution $\mathbf{X}$.

Figures 5(A) and (B) illustrate the EV trade-off diagrams for obtaining the gap anomaly estimates in Fig. 4(B) that were derived from the joint inversion of the simulated near-surface anomalies outside the gap and the Magsat anomaly simulations in Fig. 4(A). Here, the correlation coefficients

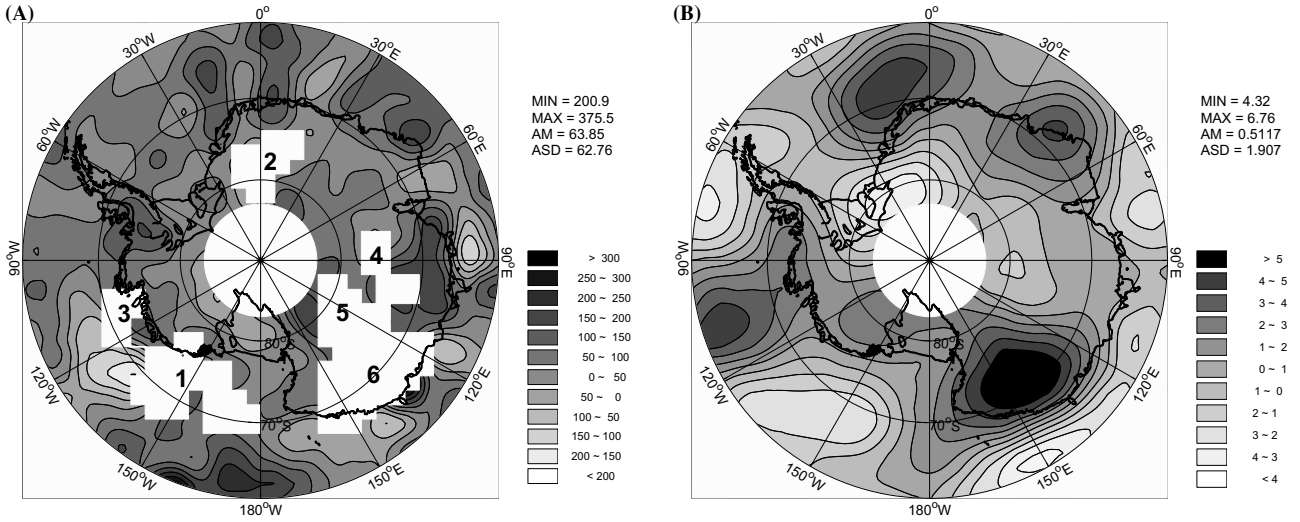

Fig. 6. (A) ADMAP magnetic anomalies at 5 km altitude low-passed filtered for 400 km and longer wavelengths. (B) Ørsted comprehensive lithospheric magnetic anomalies at 700 km (Kim, 2002).

(CC) and root-mean-square (RMS) differences from the predictions of solutions for various EV-values are compared. These results are plotted for the near-surface anomalies outside and within the gap by the solid gray and dashed black curves, respectively. In actual applications, we can only estimate the trade-off diagram for near-surface anomalies outside the gap, but these results closely mirror the performance of the solution within the gap as suggested by Fig. 5. Specifically, the Magsat data predictions in Fig. 4(B), obtained using EV $= 10^6$ as indicated by the trade-off diagram in Fig. 5(A), have minimal RMS difference and maximum CC relative to the near-surface anomalies.

The comparison of the gap predictions in Fig. 4(B) with the 'true' gap values of Fig. 3(C) is given in Table 1. These results clearly favor the use of the Magsat data over minimum curvature for estimating the gap anomalies. Relative to the minimum curvature errors, the Magsat-based prediction errors are reduced in amplitude, but higher frequency to reflect the improved phase properties of the predictions.

The measurement errors of Ørsted's magnetometers are roughly an order-of-magnitude smaller than 3 nT measurement errors of the Magsat data. Hence, we evaluated our crustal inversion model at 700 km altitude to the nearest 0.3 nT for the simulated Ørsted total field magnetic anomalies in Fig. 4(C). The simulated satellite anomalies were then combined with the near-surface anomalies outside the gap by EV-optimized joint inversion using the trade-off diagrams in Fig. 5(B).

From these trade-off diagrams in Fig. 5(B), an 'optimal' EV $= 10^4$ was selected for a solution that yielded the improved gap predictions shown in Fig. 4(D). Table 1 compares these gap predictions with the 'true' gap values of Fig. 3(C). The results strongly favor the use of the Ørsted data over the Magsat data and minimum curvature for filling in regional gaps in near-surface survey coverage.

The CHAMP satellite also carries Ørsted's magnetometers, but at significantly lower altitudes. Accordingly, Figure 4(E) gives the simulated CHAMP anomalies evaluated to the nearest 0.3 nT at 350 km altitude from our crustal magnetization model. These CHAMP anomalies were combined with near-surface anomalies outside the gap by EV-optimized joint inversion based on the trade-off diagrams in Fig. 5(C). An "optimal" EV $= 10^5$ was chosen from the trade-off diagrams for a solution that gives the significantly improved gap predictions in Fig. 4(F). Table 1 compares these gap estimates with the 'true' gap values from Fig. 3(C). These results suggest that the CHAMP lithospheric anomalies will be particularly well suited for estimating near-surface anomalies because measurement accuracy is an order-of-magnitude greater than Magsat's and the orbital altitudes are much lower than Ørsted's.

The correlation coefficients (CC) in Table 1 provide estimates of the noise content in the gap predictions using the noise (N)-to-signal (S) ratio (e.g., Foster and Guinzy, 1967; Kim, 1995) given by $(N/S) \approx [(|CC|)^{-1} - 1]^{1/2}$. Accordingly, the gap predictions from minimum curvature have a noise level of roughly 72%, while using the Ørsted data reduces the noise level to about 12%. The upper triangular portion of the four right columns in Table 1 gives the relative reductions in prediction noise for the four approaches. For example, the Ørsted-based predictions represent roughly an 83% reduction of the minimum curvature noise.

Table 1 also suggests that the new-generation satellite data offer significant advantages over the Magsat data for estimating near-surface magnetic anomalies. For example, a maximum reduction of about 70% in the noise level of the Magsat-based predictions can result with the use of the Ørsted data. This reduction reflects the order-of-magnitude increase in measurement accuracy of the Ørsted data even though they are at much higher altitudes. The use of the lower altitude, high-accuracy CHAMP lithospheric magnetic anomalies, on the other hand, can reduce noise levels in the Magsat-based predictions by roughly 90%. Hence, further significant improvements in estimating near-surface magnetic fields in unsurveyed regions can result as the accuracy in estimating the lithospheric anomalies in the lower altitude CHAMP data improves. Indeed, an extension of our analysis shows that increasing the measurement accuracy in

the magnetic observations a further order-of-magnitude (i.e., 0.03 nT) at CHAMP altitudes could reduce noise levels by a maximum of nearly 99% relative to the Magsat-based predictions. This accuracy might be realized from magnetic gradient measurements such as those to be obtained by the multi-satellite SWARM mission (Olsen *et al.*, 2004).

4. ADMAP Coverage Gap Predictions

To date, we have processed only the Magsat and Ørsted mission data fully for magnetic anomalies of the Antarctic lithosphere. For filling in coverage gaps in the ADMAP compilation of near-surface magnetic surveys shown in Fig. 2(A), the above simulations clearly favor the use of Ørsted data over the Magsat observations. Hence, in the present section, we develop near-surface anomaly estimates for the ADMAP coverage gaps from the joint inversion of the available near-surface anomalies and the comprehensive Ørsted lithospheric magnetic anomalies shown in Fig. 6(B) (Kim, 2002).

For the joint inversion, we considered the ADMAP anomalies low-pass filtered for 400 km and larger wavelengths shown in Fig. 6(A) that likely may be detected at satellite altitudes of 400 km and higher. The regional ADMAP anomalies were then resampled in spherical coordinates at roughly a 200 km interval. The resampling greatly reduced the number of ADMAP data in the analysis with essentially no loss of regional anomaly detail.

Near-surface magnetic surveys are lacking in the large numerically labeled areas in Fig. 6(A). These coverage gaps are located in on- and off-shore Marie Byrd Land (#1) and off-shore Thurston Island (#3) in West Antarctica, and east of the Shackleton Range (#2), the Aurora Subglacial Basin (#4) and in the vicinity of Wilkes Land (#5 and #6) in East Antarctica. The central void south of 83°S was not considered in our analysis because it lacks satellite coverage due to the 83° inclination of the Ørsted mission orbits.

We separately modeled each gap for a set of anomaly predictions. In each case, the inversion model consisted of 20 km thick spherical prisms with sides 150 km and tops at 30 km below sea level over the study area. The effects of these prisms for each inversion were modeled by Gauss-Legendre quadrature integration.

Figure 7 gives the "optimal" EV-values that were selected for developing the best anomaly predictions in each coverage gap. In every case, the "optimal" EV-value maximized the correlation coefficient between the inversion predictions and the observed anomaly values around the coverage gaps. Figure 8(A) gives the regional ADMAP magnetic

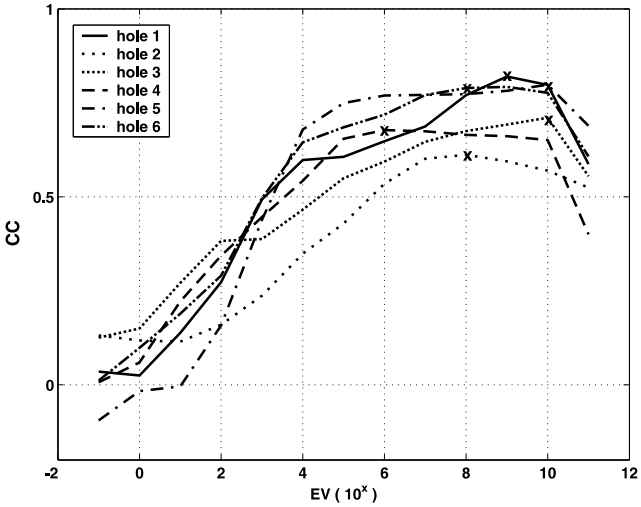

Fig. 7. Error variance (EV) spectra for the ADMAP coverage gaps or holes. The cross in each spectrum marks the 'optimal' EV-value for developing the best anomaly predictions for the corresponding gap from the joint inversion of the Ørsted and regional ADMAP anomalies.

anomalies where each coverage gap was filled by the related joint inversion using the Ørsted lithospheric anomaly data (Fig. 6(B)). For comparison, Figure 8(B) gives the gridded regional ADMAP anomalies with the coverage gaps filled in by minimum curvature that the absence of satellite magnetic data might have necessitated.

Gap #6 over Wilkes Land in East Antarctica shows the most prominent differences in the minimum curvature and the Ørsted predictions. The geological implications of the differences are difficult to assess because the region is covered by an ice sheet up to roughly 3 km thick (e.g., von Frese *et al.*, 1999b). Radar sounding data suggest that the Wilkes Subglacial Basin and its salients may constitute a major intracratonic zone of sedimentation where the edge of the basin probably marks the limit of the orogenic activity responsible for the Transantarctic Mountains (Steed and Drewry, 1982). These results also identify a probable major fault block running along longitude 135°E that correlates with a positive magnetic anomaly which is relatively subdued and broken up towards the coastline in the Ørsted-based predictions of Fig. 8(A). However, the positive anomaly in the Ørsted-based predictions tends to resolve relatively well the subglacial plateau at Dome C (75°S, 127°E). Originally discovered from seismic refraction and gravity data, the plateau is composed of crystalline bedrock covered by little or no sedimentary rock (Bentley *et al.*, 1983). Modeling of

Table 1. Performance statistics for using minimum curvature (MC in Fig. 2(D)) and Magsat (Fig. 3(B)), Ørsted (Fig. 3(D)), and CHAMP (Fig. 3(F)) magnetic anomalies to fill a simulated gap in aeromagnetic anomaly coverage. The prediction statistics include the root-mean-square (RMS) difference, the correlation coefficient (CC), and related noise (N) levels. In the right four columns, the upper triangular portion gives the relative noise reductions for the gap predictions from the various constraints.

Constraint	RMS	CC	N	MC	Magsat	Ørsted	CHAMP
MC	108.7 nT	0.34	72%	0	44%	83%	94%
Magsat	98.5 nT	0.51	40%		0	70%	90%
Ørsted	74.5 nT	0.81	12%			0	67%
CHAMP	32.1 nT	0.93	4%				0

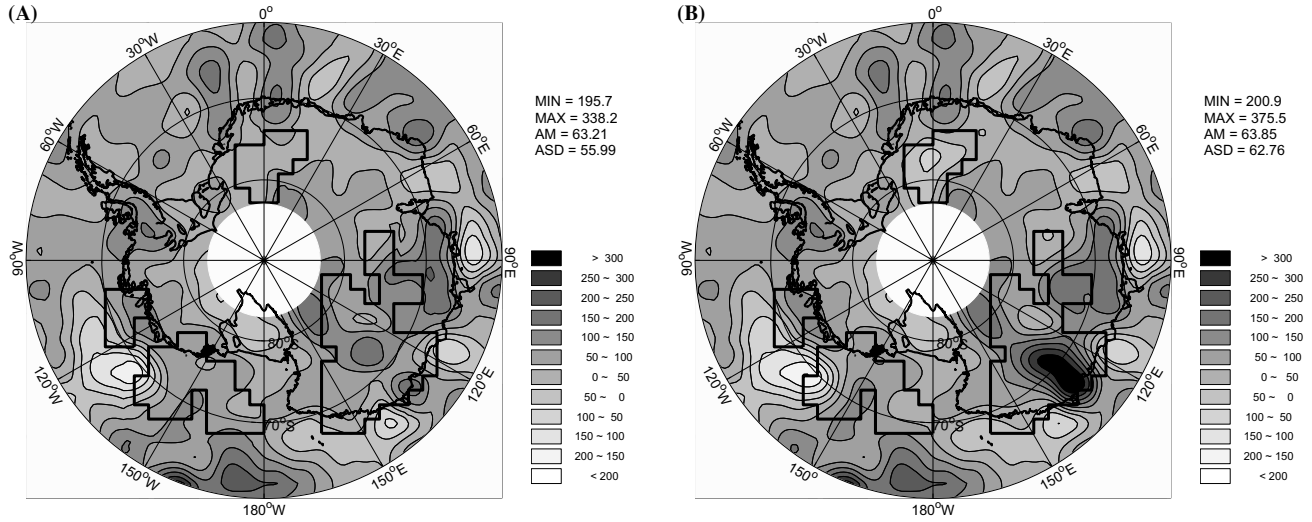

Fig. 8. (A) Regional ADMAP magnetic anomaly grid with coverage gaps filled in by joint inversion using Ørsted lithospheric anomalies at 700 km altitude. (B) Regional ADMAP magnetic anomaly grid with coverage gaps filled in by minimum curvature.

the ground-based magnetic measurements also showed that the plateau is characterized by strong positive magnetization with a Koenigsberger ratio greater than unity and hence minimal apparent remanence (Bentley *et al*., 1983).

Other gaps where the two sets of predictions are conspicuously different include gap #2 east of the Shackleton Range and gap #1 off the Marie Byrd Land coast. For gap #2, the minimum curvature predictions suggest a deep closed minimum relative to the smaller amplitude minimum that trends SW/NE through the gap in the Ørsted-based predictions. The minimum curvature predictions reflect the straightforward extrapolation of boundary observations into the gap, whereas the Ørsted-based predictions tend to honor the regional SW trend of minima outside the gap that extends to a slightly positive magnetic anomaly over the high-grade metamorphic rocks of the Shackleton Range (Hunter *et al*., 1996; Kleinschmidt and Buggisch, 1994). Additional geological implications for these predictions are difficult to develop because of the gap's ubiquitous cover of snow and ice.

Similarly, the geological implications for the predictions in gap #1 are difficult to ascertain because the gap is covered by seawater. Here, however, the minimum curvature predictions appear more strongly biased to the minima along the western boundary of gap #1 than are the Ørsted-based predictions.

According to our Weddell Sea simulations, the Ørsted-based gap predictions in Fig. 8(A) provide the best representation currently available for the 400 km and larger ADMAP components. Superposing the residual hi-cut filtered ADMAP components with wavelengths shorter than 400 km on Fig. 8(A) yields Fig. 2(B) that at present represents our best compilation of the near-surface magnetic anomalies of the Antarctic. We are currently working, however, to improve lithospheric magnetic anomaly estimates from the CHAMP magnetic and gravity observations (e.g., Kim *et al*., 2002; von Frese *et al*., 2003; Kim *et al*., 2004). Hence, further significant improvements in the gap predictions may be possible as these lithospheric magnetic anomaly estimates become available from the lower altitude CHAMP mission.

Our approach of using anomaly simulations to test the utility of satellite data for making near-surface magnetic anomaly predictions in the coverage gaps of the ADMAP compilation can be readily extended to other applications. We did not try to adjust our gap predictions for errors in the Antarctic magnetic observations because they are very poorly characterized at present. Thus, we produced gap predictions from the direct inversions of the satellite and near-surface observations. Obviously, the direct inversion biases the predictions to the near-surface or satellite anomalies and related errors where the spatial scale of the near-surface coverage gap is respectively small or large relative to the resolution limit of the satellite anomalies. However, given effective estimates of the observational errors, we can also weight the observational data sets to manage their relative contributions in making gap predictions (Ravat *et al*., 1998; 2002).

In general, our gap predictions are clearly not unique because they are based on highly simplified crustal models and imperfectly distributed and measured anomaly observations. Hence, our predictions must be used with caution for geological applications because they can only be as good as the data and assumptions used in deriving them.

5. Summary and Conclusions

The simulations show the important role that satellite magnetic observations can play in estimating magnetic anomalies in regional coverage gaps of near-surface survey compilations. Unfortunately, anomaly errors and the non-uniqueness of any continuation process profoundly limit the direct downward continuation of satellite magnetic anomalies for this application (e.g., von Frese *et al*., 2004). However, joint inversion of the satellite data and available near-surface anomalies surrounding the coverage gap can yield effective gap predictions.

As shown in Table 1, the greatly improved measurement accuracy of the Ørsted data over the Magsat data clearly favors the use of the higher altitude data for supplementing coverage gaps in the ADMAP compilation. Accordingly,

Figure 2(B) gives our best current estimate of the Antarctic near-surface magnetic anomaly field. Here, we filled the gaps in the ADMAP compilation of terrestrial, shipborne, and aeromagnetic surveys (Fig. 2(A)) with the near-surface gap predictions (Fig. 8(A)) from the joint inversion of the Ørsted lithospheric anomalies (Fig. 6(B)) and the regional ADMAP components (Fig. 6(A)).

However, further significant improvements in these near-surface estimates are likely by including the lower altitude CHAMP magnetic anomalies of the Antarctic lithosphere. By Table 1, for example, the use of the CHAMP data can reduce the noise levels in the Magsat- and Ørsted-based gap predictions by about 90% and 67%, respectively. The noise reduction relative to Magsat-based predictions simply reflects the order-of-magnitude increase in measurement accuracy of the CHAMP data, while the signal enhancement over the Ørsted-based predictions is due to the lower altitudes of the CHAMP data.

Of course, these results are limited in practice by the errors in reducing magnetic observations for their lithospheric components. These reduction errors can be especially severe in the polar regions where strong and highly dynamic external magnetic fields operate and the core field attributes are very poorly constrained. However, improving measurement accuracy can greatly facilitate the reduction of magnetic observations for non-lithospheric effects because of the enhanced correlation that can result between near-surface and satellite magnetic anomalies of the lithosphere.

Acknowledgments. This research was peformed under the auspices of the Antarctic Digital Magnetic Anomaly Project (ADMAP). We thank the members of the international working group for their contributions to ADMAP, and the International Association of Geomagnetism and Aeronomy (IAGA) and the Scientific Committee for Antarctic Research (SCAR) for supporting ADMAP. Grants from NSF-OPP (0338005) and NASA (NAG5-7645) also funded elements of this research. HRK was supported as a Goddard Visiting Fellow in the Earth Sciences by NASA Cooperative Agreement NCC5-494. We thank Mark Pilkington and an anonymous reviewer for their constructive comments on this paper. JWK was supported by National Research Lab. Project of Korea Ministry of Science and Technology (Grant # M1-0302-00-0063).

References

Alsdorf, D. E., R. R. B. von Frese, J. Arkani-hamed, and H. C. Noltimier, Separation of lithospheric, external, and core components of the south polar geomagnetic field at satellite altitudes, *J. Geophys. Res.,* **99**, 4655–4667, 1994.

Arkani-Hamed, J. and D. W. Strangway, Intermediate scale magnetic anomalies of the Earth, *Geophysics,* **50**, 2817–2830, 1985.

Arkani-Hamed, J., W. E. S. Urquhart, and D. W. Strangway, Scalar magnetic anomalies of Canada and northern United States derived from Magsat data, *J. Geophys. Res.,* **90**, 2599–2608, 1985.

Arkani-Hamed, J., R. A. Langel, and M. Purucker, Magnetic anomaly maps of Earth derived from POGO and Magsat data, *J. Geophys. Res.,* **99**, 24,075–24,090, 1994.

Arkani-Hamed, J., J. Verhoef, W. Roest, and R. Macnab, The intermediate wavelength magnetic anomaly maps of the North Atlantic ocean derived from satellite and shipborne data, *Geophys. J. Int.,* **123**, 727–743, 1995.

Briggs, I. C., Machine contouring using minimum curvature, *Geophysics,* **39**, 39–48, 1974.

Bentley, C. R., S. Shabtaie, C. S. Lingle and D. D. Blankenship, Analysis of geophysical data from Dome C and the Ross Ice Shelf, *Antarctic Journal of U. S.*, **18**, 104–105, 1983.

Cohen, Y. and J. Achache, New global vector magnetic anomaly maps derived from Magsat data, *J. Geophys. Res.,* **95**, 10783–10800, 1990.

Dampney, C. N., The equivalent source technique, *Geophysics,* **45**, 39–53, 1969.

Foster, M. R. and N. J. Guinzy, The coefficient of coherence: Its estimation and use in geophysical prospecting, *Geophysics,* **32**, 602–616, 1967.

Golynsky, A., M. Chiappini, D. Damaske, F. Ferraccioli, J. Ferris, C. Finn, M. Ghidella, T. Ishihara, A. Johnson, H. R. Kim, L. Kovacs, J. LaBrecque, V. Masolov, Y. Nogi, M. Purucker, P. Taylor, and M. Torta, ADMAP—Magnetic anomaly map of the Antarctic, 1:10,000,000 scale map, *BAS (Misc) 10*, 2002.

Grauch, V. J. S., Limitations on digital filtering of the DNAG magnetic data set for the conterminous U.S., *Geophysics,* **62**, 1281–1296, 1993.

Hildenbrand, T. G., R. J. Blakely, W. J. Hinze, R. Keller, R. A. Langel, M. Nabighian, and W. Roest, Aeromagnetic survey over U.S. to advance geomagnetic research, *Eos,* **77**, 265, 268, 1996.

Hunter, R. J., A. C. Johnson, and N. D. Aleshkova, Aeromagnetic data from the southern Weddell Sea embayment and adjacent areas: Synthesis and interpretation, in *Geological Soceity Special Publication*, edited by B. Story, E. C. King, and R. A. Livermore, Volume 108, pp. 143–154, The Geological Society, 1996.

Kim, H. R., Antarctic lithospheric anomalies from Ørsted satellite and near-surface magnetic observations, Ph. D. thesis, The Ohio State University, Columbus, Ohio, pp. 160, 2002.

Kim, H. R., L. R. Gaya-Pique, R. R. B. von Frese, P. T. Taylor, and J. W. Kim, CHAMP magnetic anomalies of the Antarctic Crust, in *Earth Observation with CHAMP: Results from Three Years in Orbit*, edited by C. Reigber, H. Lühr, P. Schwintzer, and J. Wickert, Heidelberg: Springer-Verlag, pp. 261–266, 2004.

Kim, J.-H., Improved recovery of gravity anomalies from dense altimeter data, Ph. D. thesis, The Ohio State University, Columbus, Ohio, 1995.

Kleinschmidt, G. and W. Buggisch, Plate tectonic implications of the structure of the Shackleton Range, Antarctica, *Polarforschung,* **63**, 9–32, 1994.

Ku, C. C., A direct computation of gravity and magnetic anomalies caused by 2- and 3-dimensional bodies of arbitrary shape and arbitrary magnetic polarization by equivalent point method and a simplified cubic spline, *Geophysics,* **42**, 610–622, 1977.

Langel, R. A., Global magnetic anomaly maps derived from POGO spacecraft data, *Phys. Earth Planet. Int.,* **62**, 208–230, 1990.

Langel, R. A. and W. J. Hinze, *The Magnetic Field of the Earth's Lithosphere*, Cambridge, New York, 1998.

Langel, R. A., J. D. Phillips, and R. J. Horner, Initial scalar magnetic anomaly map from Magsat, *Geophys. Res. Lett.,* **9**, 269–272, 1982.

Li, Y. and D. W. Oldenburg, Joint inversion of surface and three-component borehole magnetic data, *Geophysics,* **65**, 540–552, 1999.

Maus, S., M. Rother, R. Holme, H. Lühr, N. Olsen, and V. Haak, First scalar magnetic anomaly map from CHAMP satellite data indicates weak lithospheric field, *Geophys. Res. Lett.,* **29**, 10.1029/2001GL013685, 2002.

Mayhew, M. A., An equivalent layer magnetization model for the United States derived from satellite altitude magnetic anomalies, *J. Geophys. Res.,* **87**, 4837–4845, 1982.

Olsen, N., T. Sabaka, and L. Tøffner Clausen, Determination of the IGRF 2000, *Earth Planets Space,* **52**, 1175–1182, 2000.

Olsen, N., E. Friis-Christensen, G. Hulot, M. Korte, A. Kuvshinov, V. Lesur, H. Lühr, S. Macmillan, M. Mandea, S. Maus, M. Purucker, C. Reigber, P. Ritter, M. Rother, T. Sabaka, P. Tarits, and A. Thomson, Swarm-End-to-End mission performance simulator study, DSRI Report 1/2004: ESA contract No. 17263/03/NL/CB, 2004.

Pilkington, M. and W. R. Roest, An assessment of long-wavelength magnetic anomalies over Canada, *Can. J. Earth Sci.,* **31**, 12–23, 1996.

Purucker, M. E., T. J. Sabaka, and R. A. Langel, Conjugate gradient analysis: A new tool for studying satellite magnetic data sets, *Geophys. Res. Lett.,* **23**, 507–510, 1996.

Ravat, D. N., W. J. Hinze, and R. R. B. von Frese, Lithospheric magnetic property contrasts within the South American plate derived from damped least-squares inversion of satellite magnetic data, *Tectonophysics,* **192**, 159–168, 1991.

Ravat, D. N., R. A. Langel, M. Purucker, J. Arkani-Hamed, and D. E. Alsdorf, Global vector and scalar Magsat magnetic anomaly maps, *J. Geophys. Res.,* **100**, 20111–20136, 1995.

Ravat, D. N., M. Pilkington, M. Purucker, T. Sabaka, P. T. Taylor, R. R. B. von Frese, and K. A. Whaler, Recent advances in the verification and geologic intgerpretation of satellite-altitude magnetic anomalies, 68th Annual Meeting, Society of Exploration Geophysicists, Expanded Abstracts, 507–510, 1998.

Ravat, D. N., K. A. Whaler, M. Pilkington, T. J. Sabaka, and M. Purucker, Compatibility of high-altitude aeromagnetic and satellite-altitude magnetic anomalies over Canada, *Geophysics,* **67**, 546–554, 2002.

Regan, R. D., J. C. Cain, and W. M. Davis, A global magnetic anomaly map, *J. Geophys. Res.,* **80**, 794–802, 1975.

Schnetzler, C. C., P. T. Taylor, R. A. Langel, W. J. Hinze, and J. D. Phillips, Comparison between the recent U.S. composite magnetic anomaly map and Magsat anomaly data, *J. Geophys. Res.,* **90**, 2543–2548, 1985.

Sexton, J. L., W. J. Hinze, R. R. B. von Frese, and L. W. Braile, Long-wavelength aeromagnetic anomaly map of the conterminous United States, *Geology,* **10**, 364–369, 1982.

Smith, W. H. F. and P. Wessel, Gridding with continuous curvature splines in tension, *Geophysics,* **55**, 293–305, 1990.

Steed, R. H. C. and D. J. Drewry, Radio echo sounding investigations of Wilkes Land, Antarctica, pp. 969–975, Univ. of Wisconsin Press, Madison, 1982.

Stroud, A. H. and D. Secrest, *Gaussian Quadrature Formulas*, Prentice-Hall, Englewood Cliffs, NJ, 1966.

Taylor, P. T., J. J. Frawley, H. R. Kim, R. R. B. von Frese, and J. W. Kim, Comparing Magsat, Ørsted and CHAMP crustal magnetic anomaly data over the Kursk Magnetic Anomaly, Russia, in *First CHAMP Mission Results for Gravity, Magnetic and Atmospheric Studies*, edited by C. Reigber, H. Lühr, and P. Schwintzer, Heidelberg: Springer-Verlag, pp. 302–308, 2003.

von Frese, R. R. B., CORRECTION to von Frese, R. R. B., W. J. Hinze and L. W. Braile, Spherical earth gravity and magnetic anomaly analysis by equivalent point source inversion (*Earth Planet. Sci. Lett.*, 53, 69–83, 1981), *Earth Planet. Sci. Lett.,* **163**, 409–411, 1998.

von Frese, R. R. B., W. J. Hinze, and L. W. Braile, Spherical-Earth gravity and magnetic anomaly modeling by Gauss-Legendre quadrature integration, *J. Geophys.,* **49**, 234–242, 1981a.

von Frese, R. R. B., W. J. Hinze, L. W. Braile, and A. J. Luca, Spherical earth gravity and magnetic anomaly analysis by equivalent point source inversion, *Earth Planet. Sci. Lett.,* **53**, 69–83, 1981b.

von Frese, R. R. B., W. J. Hinze, J. L. Sexton, and L. Braile, Verification of crustal component in satellite magnetic data, *Geophys. Res. Lett.,* **9**, 293–295, 1982.

von Frese, R. R. B., D. N. Ravat, W. J. Hinze, and C. A. McGue, Improved inversion of geopotential field anomalies for lithospheric investigations, *Geophysics,* **53**, 375–385, 1988.

von Frese, R. R. B., H. R. Kim, L. Tan, J. W. Kim, P. T. Taylor, M. E. Purucker, D. E. Alsdorf, and A. J. Anderson, Satellite magnetic anomalies of the Antarctic crust, *Annali di Geofisica,* **42**, 293–307, 1999a.

von Frese, R. R. B., L. Tan, J. W. Kim, and C. R. Bentley, Antarctic crustal modeling from the spectral correlation of free-air gravity anomalies with the terrain, *J. Geophys. Res.,* **104**, 25275–25297, 1999b.

von Frese, R. R. B., H. R. Kim, J. W. Kim, and P. T. Taylor, CHAMP, Ørsted and Magsat magnetic anomalies of the Antarctic lithosphere, in *First CHAMP Mission Results for Gravity, Magnetic and Atmospheric Studies*, edited by C. Reigber, H. Lühr, and P. Schwintzer, Heidelberg: Springer-Verlag, pp. 309–314, 2003.

von Frese, R. R. B., H. R. Kim, P. T. Taylor, and M. F. Asgharzadeh, Reliability of CHAMP anomaly continuation, in *Earth Observation with CHAMP: Results from Three Years in Orbit*, edited by C. Reigber, H. Lühr, P. Schwintzer and J. Wickert, Heidelberg: Springer-Verlag, pp. 287–292, 2004 (in press).

Whaler, K. A., Downward continuation of Magsat lithospheric anomalies to the Earth's surface, *Geophys. J. Int.,* **116**, 267–278, 1994.

H. R. Kim (e-mail: kimhr@core2.gsfc.nasa.gov), R. R. B. von Frese, A. V. Golynsky, P. T. Taylor, and J. W. Kim